



# Numerical and experimental study of the temperature field evolution of Mg alloy during high power diode laser surface melting



Yu Gan<sup>a,b</sup>, Wenxian Wang<sup>a,b,\*</sup>, Zeqin Cui<sup>a,b</sup>, Xinggui Yan<sup>a,b</sup>, Zhuosen Guan<sup>a,b</sup>, Bingshe Xu<sup>a,b</sup>

<sup>a</sup> College of Material Science and Engineering, Taiyuan University of Technology, Taiyuan 030024, Shanxi, China

<sup>b</sup> Key Laboratory of Interface Science and Engineering in Advanced Materials of Ministry of Education, Taiyuan 030024, Shanxi, China

## ARTICLE INFO

### Article history:

Received 29 January 2014

Accepted 9 February 2015

### Keywords:

Laser surface melting

Temperature field

Finite element simulation

AZ31B magnesium alloy

## ABSTRACT

During the laser surface melting (LSM) of AZ31B Mg alloy, obtaining desired temperature field distribution is essential for production goal and reliable service performance. In this study, a 3D finite element model was developed to analyze the thermal characteristics during the diode laser surface melting of Mg alloy with different process parameters. The simulation visually predicts the great temperature gradient and fast cooling speed during LSM. The microstructure of the fusion zone was observed to validate the accuracy of the simulation. Verification experiment based on infrared temperature measurement (ITM) was applied. By comparing the maximum temperature values, the average heating and cooling rate and the dimension of the melt pool with various laser powers and scanning speed, the simulation results are in good agreement with the experimental measurements.

© 2015 Elsevier GmbH. All rights reserved.

## 1. Introduction

A major concern in Mg surface modification is to achieve surface strengthening by reducing micro-segregation and microstructure refinement [1]. During the LSM of Mg alloy, the thermal field plays an important role in determining microstructures and surface performance [2–4]. The process parameters such as laser spot size, laser power, scanning speed, and scanning strategy all play crucial roles on the development of temperature gradients and the morphology of the melt pool [5,6]. However, due to the extremely numerous data involved in SLM process, it can be time-consuming and costly through experiments for detailed investigation [7]. As such, a comprehensive study of numerical simulation has been undertaken as an optimization on the temperature field distribution, residual stress and other thermal mechanisms [8–10].

To date, an impressive amount of research on this topic has been carried out. By developing a numerical model to account for the non-equilibrium solidification in the melt pool, numerical modeling of heat and mass transfer in laser surface alloying was introduced by Chakraborty [11]. A mathematical model was

formed to conduct numerical simulation of temperature field and weld pool dimensions for the novel high power direct-diode laser (HPDDL) welding process by Wu and Wang et al. [12]. Hussein et al. [13] developed a finite element simulation of the temperature and stress fields in single layers built without support in selective laser melting. Kong et al. [14] focused on investigating the temperature gradient in the HAZ by regulating the scanning speed of the laser beam reported recently. In order to study the heat transfer from the laser keyhole to the weld pool and details of the fluid flow, a numerical and experimental study of molten pool formation was carried out by Abderrazak and Bannour et al. [15].

With the development of the diode laser, it has become a undoubtedly optimal choice for scientists and engineers because of its high efficiency and simple operation [16]. In this study, both numerical and experimental studies of high power diode laser surface melting AZ31B Mg alloy were carried out. Moving heat source and boundary conditions were accomplished by a user written subroutine implemented in ANSYS parametric design language (APDL). The verification experiment based on infrared temperature measurement was carried out for contrastive analysis [17,18].

## 2. Finite element model

The dimension of AZ31B magnesium alloy sample used in this work was 60 mm × 40 mm × 10 mm. Just a half of the sample was analyzed because of the symmetrical distribution. Considering the

\* Corresponding author at: Taiyuan University of Technology, College of Materials Science and Engineering, 79 No. Yingze Street, Taiyuan 030024, Shanxi, China. Tel.: +86 6010076; fax: +86 6010076.

E-mail addresses: [wangwenxian@tyut.edu.cn](mailto:wangwenxian@tyut.edu.cn), [m36helen@163.com](mailto:m36helen@163.com) (W. Wang).

**Table 1**  
High heat physical properties of AZ31B magnesium alloy.

| Temperature $T$ (K) | Density $\rho$ (kg/m <sup>3</sup> ) | Specific heat capacity $C$ [J/(kg K)] | Heat conductivity factor [W/(m K)] | Convection motion |
|---------------------|-------------------------------------|---------------------------------------|------------------------------------|-------------------|
| 293                 | 1780                                | 1050                                  | 96.4                               | 62.3              |
| 373                 | 1780                                | 1130                                  | 101                                | 62.3              |
| 473                 | 1780                                | 1170                                  | 105                                | 62.3              |
| 573                 | 1780                                | 1210                                  | 109                                | 62.3              |
| 673                 | 1780                                | 1260                                  | 113                                | 62.3              |
| 905                 | 1780                                | 1300                                  | 150                                | 62.3              |

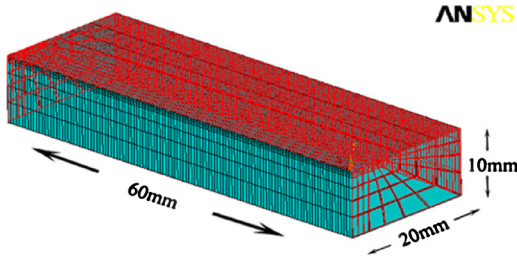


**Fig. 1.** Three-dimensional entity element of the conditions of the model additional border.

precision and time consumption in the calculation, the 3D finite element analysis (FEA) model establishment is shown in Fig. 1. The material thermal physical property parameters such as specific heat capacity, density, heat conductivity factor etc. were inputted at the same time, as listed in Table 1.

2.1. Heat source modeling

Unlike other energy sources, the diode laser is characterized with a rectangular beam of which the spot size is 6 mm × 2 mm. The uniform energy distribution can be described as:

$$q(x, y, z) = \begin{cases} \frac{\eta P}{DH} & x = L_w, |y - y_0| \leq \frac{D}{2}, vt < x < vt + H, \\ \text{other} & \end{cases} \quad (1)$$

where  $\eta$  is the absorption efficiency of laser by the material.  $y_0$  is location of laser beam center along the  $y$ -axis.  $P$  is the laser power,  $L_w$  is the thickness of the sample,  $D$  is the focused laser beam length,  $H$  is the focused laser beam width,  $t$  is the time, and  $v$  is the laser scanning speed.

According to the disperse theory of finite element method, small intermittent jump moving heat source was applied to simulate the continuous laser scanning. Therefore, the heat source movement can be achieved by cyclic loading.

2.2. Thermal conductivity and boundary conditions

The temperature variation during the SLM process is a highly nonlinear change, the heat equilibrium satisfies the following equation:

$$c(T) \rho(T) \frac{\partial T}{\partial t} = \frac{\partial}{\partial x} \left[ k(T) \frac{\partial T}{\partial x} \right] + \frac{\partial}{\partial y} \left[ k(T) \frac{\partial T}{\partial y} \right] + \frac{\partial}{\partial z} \left[ k(T) \frac{\partial T}{\partial z} \right] + Q \quad (2)$$

where  $k(T)$ ,  $c(T)$ ,  $\rho(T)$  are the factors of thermal conductivity, specific heat capacity, density respectively;  $T$  is temperature and  $Q = (x, y, z, t)$  is the volumetric heat generation (W/m<sup>3</sup>).

The moment when the heat and mass transfer effect takes place is defined as the initial time. The top surface boundary conditions include the heat losses due to the convection, radiation and heat input from the moving heat source as given by

$$k(T) \frac{\partial T}{\partial z} = q(x, y, z) - \sigma \varepsilon (T^4 - T_\infty^4) - h_c (T - T_\infty) \quad (3)$$

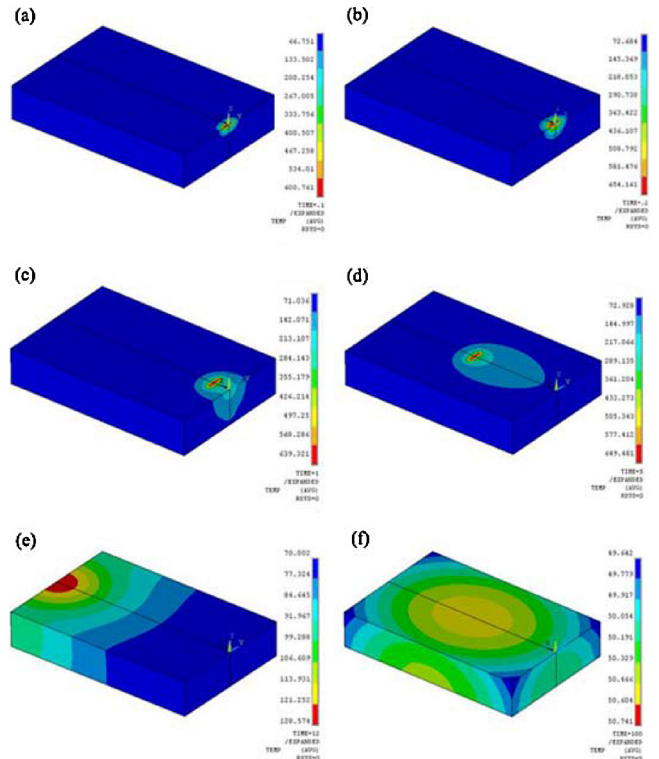


**Fig. 2.** Surface temperature field distributions during LSM process (a) 0.1 s (b) 0.2 s (c) 1 s (d) 5 s (e) 12 s (f) 100 s.

where  $q(x, y, z)$  is the heat input from laser radiation,  $\sigma$  is the Stefan–Boltzman constant,  $\varepsilon$  is emissivity,  $T_\infty$  is the room temperature, and  $h_c$  is the forced convection coefficient due to the shielding gas.

And the boundary conditions on other surfaces,

$$-k(T) \frac{\partial T}{\partial n} = \sigma \varepsilon (T^4 - T_\infty^4) + h_c (T - T_\infty) \quad (4)$$

here  $n$  is the normal outward vector to the surface of specimen.

2.3. Temperature field distribution

During the LSM process, the temperature of the sample is elevated rapidly under the direct irradiation of laser beam. And the thermal conduction caused by the absorbed energy forms quasi-stable temperature fields. A thermal analysis, shown in Fig. 2, demonstrates the temperature evolution during the LSM of Mg alloy with a direct diode laser power of 2000 W and scanning speed of 360 mm/min. As the laser beam moves along the track, the temperature profile changes accordingly from the beginning to the end of the heating process shown in Fig. 2(a)–(f). The shape of the temperature field typically presents a trailing-comet shape. Because of the 6 mm × 2 mm rectangular laser spot, the top surface of the Mg sample is quickly heated and generates a narrow laser-material interaction zone. It is further observed that the temperature

Download English Version:

<https://daneshyari.com/en/article/848563>

Download Persian Version:

<https://daneshyari.com/article/848563>

[Daneshyari.com](https://daneshyari.com)